Journal of Geophysical Research: Solid Earth

Supporting Information for

Seismic Structure of the Lithosphere-Asthenosphere System Beneath the Oldest Seafloor Revealed by Rayleigh-Wave Dispersion Analysis

Yuki Kawano[1], Takehi Isse[1], Akiko Takeo[1], Hitoshi Kawakatsu[1,2], Manabu Morishige[1], Hajime Shiobara[1], Nozomu Takeuchi[1], Hiroko Sugioka[3], YoungHee Kim[4], Hisashi Utada[1], and Sang-Mook Lee[4]

[1]Earthquake Research Institute, The University of Tokyo, Tokyo, Japan

[2]Institute of Earth Sciences, Academia Sinica, Taipei, Taiwan

[3]Graduate School of Science, Kobe University, Hyogo, Japan

[4]School of Earth and Environmental Sciences, Seoul National University, Seoul, Republic of Korea

Corresponding author: Takehi Isse (tisse@eri.u-tokyo.ac.jp)

Contents of this file

Text S1. The initial crustal structure

The initial crustal structure is fixed to the results of seismic reflection surveys of Abrams et al. (1993). In Abrams et al. (1993), the Vp depth profiles are obtained by sonobuoys at an area covering the Oldest-1 Array. We set the average profile derived from sonobuoy 4m, 8m, and 21 as the initial profile for the eastern area, whereas we set the average profile derived from sonobuoy 8 and 18 as the initial profile for the western area. The thickness for each layer is fixed throughout the inversion.

Text S2. The numerical simulation for the development of azimuthal anisotropy due to seafloor spreading near a RRR triple junction

We model seismic azimuthal anisotropy pattern due to the LPO of olivine and enstatite during the evolution of three plates from a ridge-ridge-ridge triple junction. The model domain size is 200 km in depth and 1500 × 1500 km horizontally. The angle between the ridge axes is 120˚ and the spreading rate of the three plates is constant as 1 cm/year. The thermal structure is given by half-space cooling model. The mantle flow is driven solely by the imposed spreading rate (i.e., passive upwelling) and it is computed assuming temperature-dependent viscosity as in, for example, Shen and Forsyth (1992). The method to predict LPO and the resultant seismic anisotropy follows Morishige and Honda (2011, 2013). A-type olivine fabric is assumed, and the volume fractions of olivine and enstatite are set as 70 % and 30 %, respectively. The crystals initially have random orientations at 180 km depth. As materials flow, the development of LPO of crystal aggregates is traced along a streamline from 180 km depth to a target position based on the model by Kaminski et al. (2004). Then, using the obtained LPO at the target position and the experimentally derived elastic tensor of a single crystal, the elastic tensor of a polycrystalline is obtained by Voigt average. Assuming vertically incident S-waves, the fast and slow velocities ($V_{S,slow}$ and $V_{S,fast}$) and corresponding polarization directions are calculated from the elastic tensor by solving the Christoffel equation. Then, azimuthal anisotropy is obtained as $2(V_{S,fast} - V_{S,slow})/(V_{S,fast} + V_{S,slow})$ with the fast direction along the polarization direction of the fast S-wave.

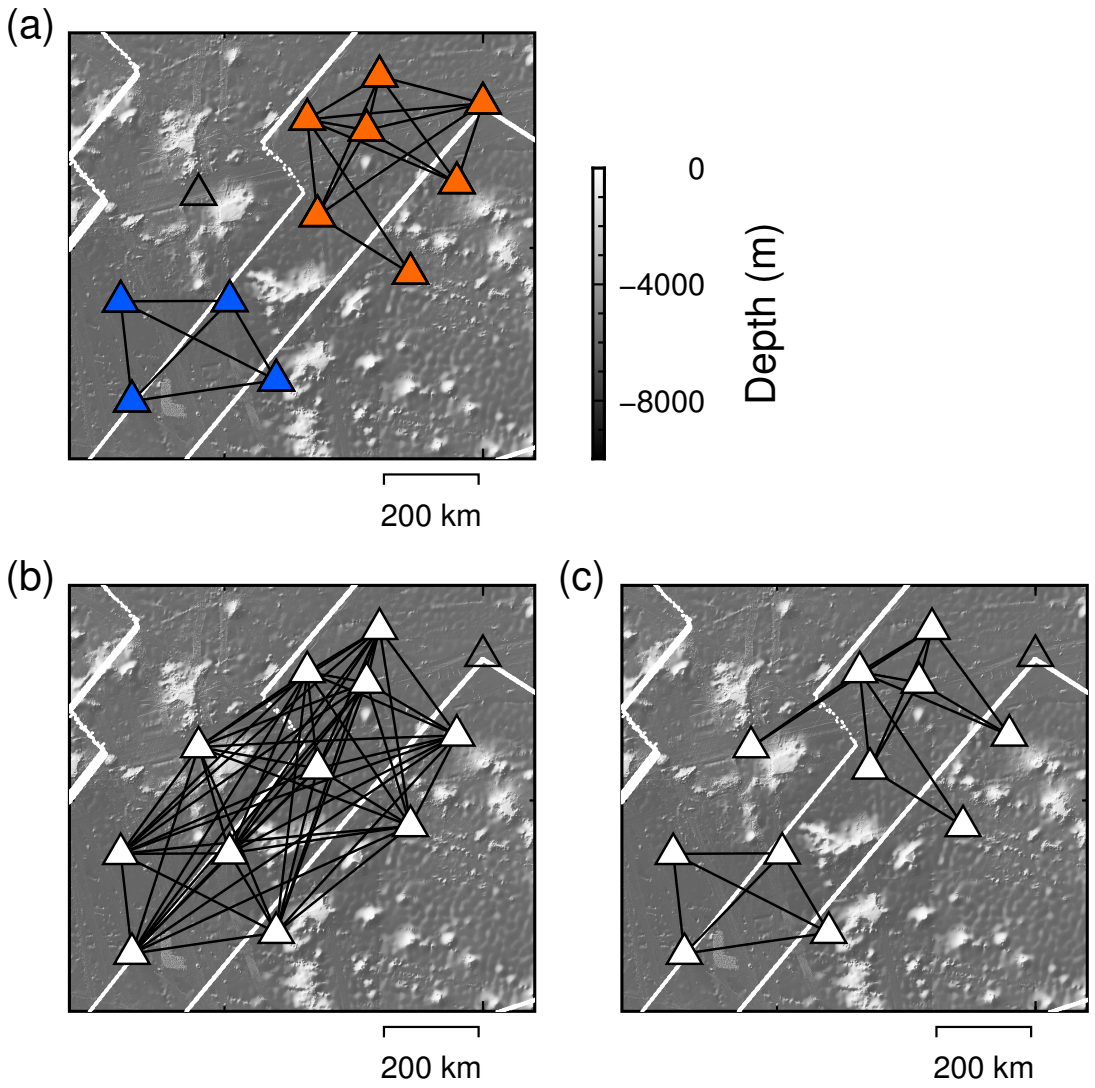

Figure S1. (a) Station pairs used for the ambient noise analysis. Blue and orange triangles are the stations of the western and the eastern areas of the array, respectively. Station pairs used in the analysis in each area are connected by black solid lines. The open triangle represents the station that is not used in the analysis. (b, c) Station pairs used for the teleseismic waveform analysis in period ranges of 40–200 s (b) and 25–40 s (c). Station pairs used in the analysis are connected by black solid lines. The white-filled triangles are stations with BBOBSs, and the open triangle is the station with DPG only, which is not used in the analysis. The background white lines represent the seafloor age isochrons (Seton et al., 2020).

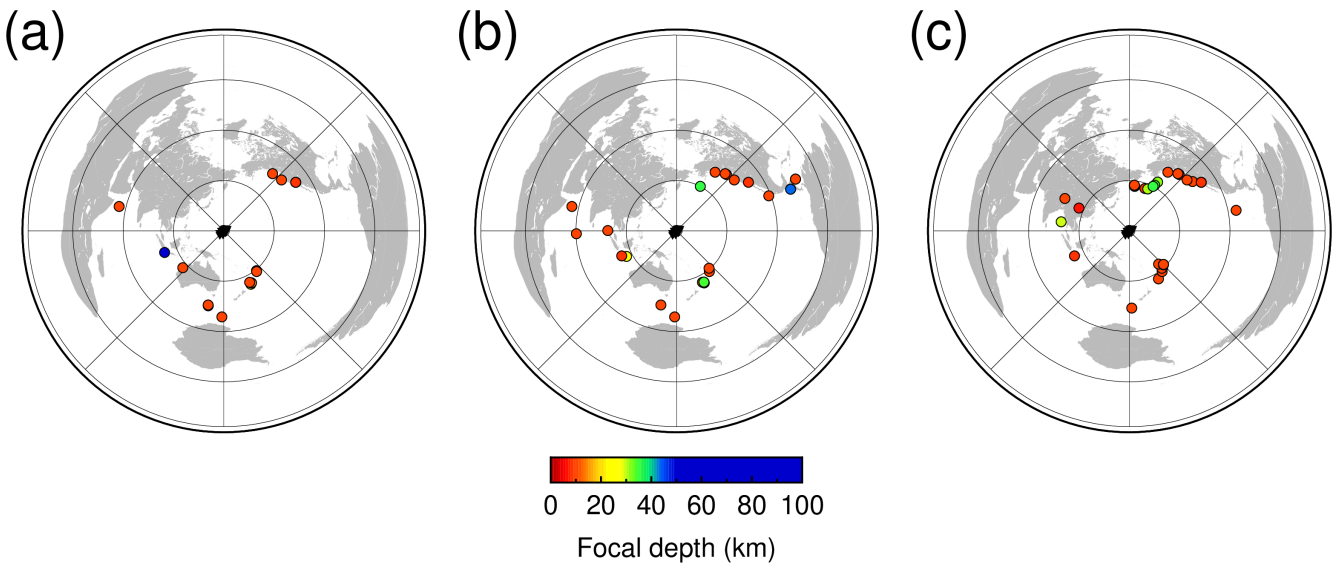

Figure S2. Epicentral distribution map of teleseismic events used in this study. The circles show the epicenters. Events are used for analysis in period ranges of (a) 100–200 s, (b) 40–100 s, and (c) 25–40 s.

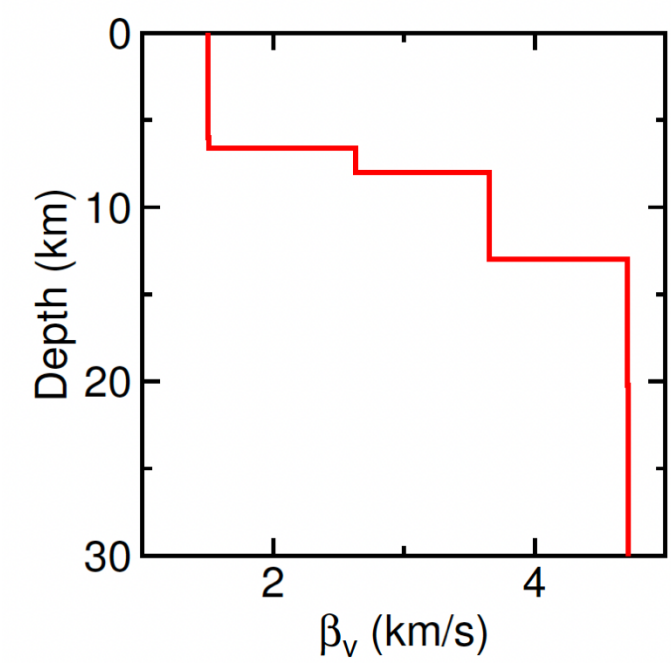

Figure S3. The crust and uppermost mantle structure that are used for the measurements at the long period bands.

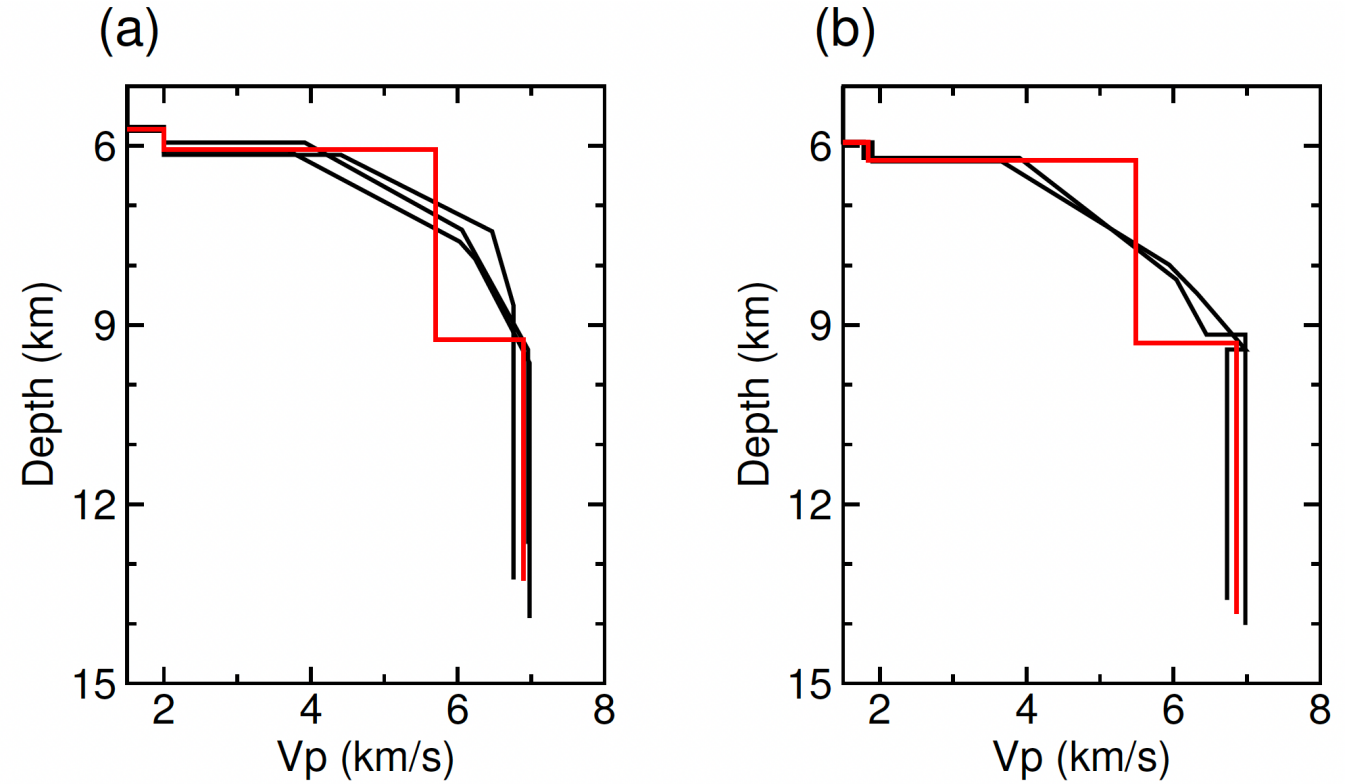

Figure S4. Initial crustal structure (red lines) for the eastern (a) and western (b) area of the Oldest-1 Array. The black lines represent the Vp depth profiles of Abrams et al. (1993).

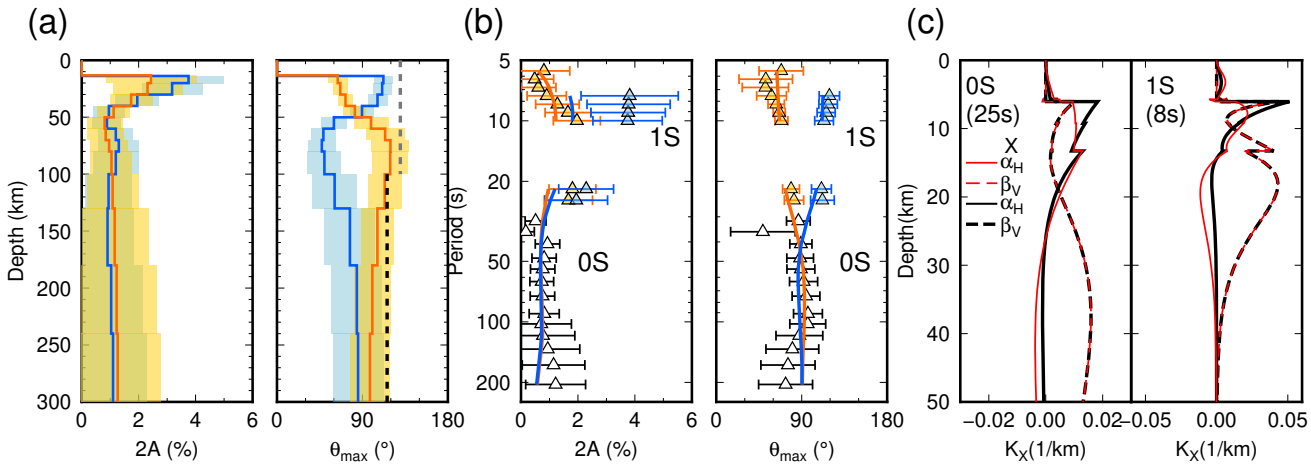

Figure S5. The azimuthal anisotropy model based on the conventional parameters (a, b), and a comparison of the sensitivity kernels (c). (a) and (b): Similar to Figure 5 (a) and (b) respectively, but for the conventional model parameterization using α_H, β_V, η. (a) The azimuthally anisotropy model profiles of β_V. The shaded areas represent the one-sigma model uncertainties. The gray and black broken lines respectively represent the direction perpendicular to the 170-Ma isochrone of Seton et al. (2020) and the current absolute plate motion direction. (b) The measurements (triangles with one-sigma error bars) and model predictions (solid lines) of azimuthal anisotropy as a function of frequency in terms of the peak-to-peak amplitude ($2A$) and the fast direction (θ_{max}) in the western (blue) and eastern (orange) arrays. Solid lines are predictions calculated from the models in (a). (c) 0S and 1S sensitivity kernels of α_H(sold lines) and β_V(broken lines) based on η_κ (black lines) and η (red lines) at periods of 25 s and 8 s, respectively. The significant difference can be seen in sensitivity kernels of α_H caused by contamination of β_V sensitivity (Kawakatsu, 2016b; Kawakatsu, 2022). This makes fitting to the peak-to-peak amplitude ($2A$) of 1S phase velocities worse in western array shown in (b).

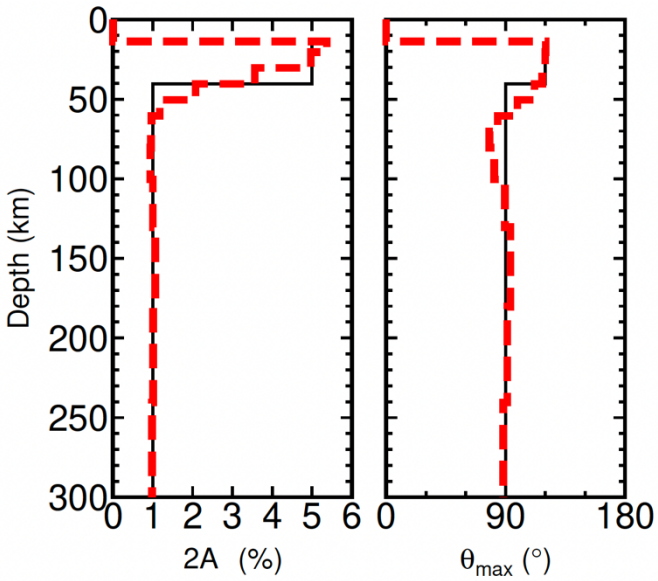

Figure S6. A synthesis test of the inversion method for the azimuthal anisotropy. The input (black line) and the retrieved (thick dashed red line) model profiles of β_V. The synthesis test is performed under the same parameters, such as the scaling among velocity parameters and the vertical smoothing between the neighboring layers, as in Figure 5. The test result indicates that when there is a discontinuous change in azimuthal anisotropy between the shallow and deep depths, the inverted model shows an overshoot of fast-axis at depths below the discontinuity (between 60 and 120 km). Except for the depth range, the input model is well recovered.